Charge stability of a triple quantum dot with a finite tunnel coupling

Soo-Young Lee[1,2] and Yunchul Chung[2,*]

[1]*Max Planck Institute for the Physics of Complex Systems, Nöthnitzer Str. 38, D01187 Dresden, Germany*

[2]*Department of Physics, Pusan National University, Busan 609-735, Korea*

(Received 16 April 2012; revised manuscript received 13 November 2012; published 3 January 2013)

We study charge stability of a symmetric triple quantum dot by using the Hund-Milliken method. As the interdot tunnel coupling increases from zero, the stability deviates continuously from that of the capacitance model. We demonstrate how the stability diagram is modified by the tunneling coupling, especially, around the sextuple point. It is shown that the characteristic feature of the sextuple point, omnidirectional charge transport, is maintained even though the sixfold degeneracy is lifted by the tunnel coupling. This is possible because the ground state near the broken sextuple point shows election or hole delocalization over the three quantum dots.

DOI: 10.1103/PhysRevB.87.045302 PACS number(s): 73.21.La, 71.10.−w, 73.23.Hk

I. INTRODUCTION

Quantum-dot system is an ideal playground for testing quantum phenomena, since the system can be well described by quantum mechanics and its properties are quite independent of the choice of material parameters. In addition, its quantum property can be easily tuned electrostatically by adjusting the voltages on the gates. Due to such advantages, various quantum-dot systems have been extensively studied for last several decades in order to understand many intriguing phenomena including Coulomb blockade,[1–3] Kondo effect,[4] etc.

Recently, a multiple quantum dot has attracted much attention due to its application to a quantum bit (qubit) by exploiting entangled states. It has been theoretically suggested that the spin-entangled state formed in a double-dot system can be used as a quantum bit.[5] In fact, successful realization and manipulation of one and two qubits in a quantum dot system have been demonstrated.[6–9] Apart from the qubit application, double-dot systems have been taken to study charge sensing and charge delocalization,[10,11] Kondo effect,[12] etc. More exotic many body effects can occur in a triple quantum dot due to the variety of geometrical arrangement. Indeed, the triple-dot system has been studied theoretically in connection with dark state,[13,14] two-channel Kondo,[15] and so on.[16–19] Also, some experimental works have been performed to study charge rectifying,[20,21] Aharonov-Bohm effect,[22] charge stability,[23–25] etc.

The capacitance model[26] is widely used to understand the charge configuration, i.e., the number of electrons in each dot, in the multidot system. Even though the model is based on a classical capacitor circuit, the result is surprisingly useful to analyze experimental data. However, the model does not incorporate the tunnel coupling between quantum dots. Recently, the charge stability in double-dot systems with a finite tunnel coupling has been studied[27,28] by mapping the system into the Hubbard model. The tunnel-coupling effect is now well understood for double-dot systems. However, not much work has been done on the charge stability of a triple quantum-dot system with a finite tunnel coupling. Moreover, in the recent experiment with a symmetric triple dot,[29] the sextuple point (or charge frustrated state) has been observed. Due to the sixfold degeneracy, the omnidirectional charge transfer is possible at the point. It might be, therefore, interesting to ask if the sextuple point would survive the interdot tunnel interaction.

In this paper, we study the effect of the interdot tunnel coupling on the charge stability diagram of a triple-dot system, based on the Hund-Milliken method.[30,31] We focus on a symmetric triple quantum dot to study the ground-state property near the sextuple point. As the tunnel coupling increases from zero, the stability diagram exhibits a continuous deviation from the classical result given by the capacitance model. It is found that, although the degeneracy of sextuple point is lifted by the tunnel coupling, there still exists so-called a quasisextuple point where an electron and a hole are delocalized evenly over three dots. Therefore the feature of omnidirectional transfer is still maintained through these delocalized ground states at the quasisextuple point. Although we do not consider spin of electron in the model, our formalism can easily incorporate the spin effect.

II. SINGLE ELECTRON STATES

Let us consider a single electron in a triple dot. The electron is described by the single-electron Hamiltonian,

$$\hat{h}(\mathbf{x}) = -\frac{\hbar^2}{2m^*}\nabla^2 + V(\mathbf{x}), \tag{1}$$

where m^* is the effective mass of electron. $V(\mathbf{x})$ is the electric potential of triple-well type, we assume that each well has a parabolic minimum, and the depth of each minimum can be adjusted by the corresponding gate voltage V_i.

Then, the single-electron Hamiltonian matrix can be written as

$$\mathbf{H}^{(1)} = \begin{pmatrix} E_1 & t_{12} & t_{13} \\ t_{12} & E_2 & t_{23} \\ t_{13} & t_{23} & E_3 \end{pmatrix}, \tag{2}$$

where we take the orthonormal basis set $\{|\Phi_i\rangle\}$ (see Appendix A).[32,33] The diagonal element $E_i = \langle\Phi_i|\hat{h}(\mathbf{x})|\Phi_i\rangle$ is the energy of the local state $|\Phi_i\rangle$ in dot-i or, equivalently, the chemical potential μ_i of dot-i. The off-diagonal element $t_{ij} = \langle\Phi_i|\hat{h}(\mathbf{x})|\Phi_j\rangle$ is the tunnel-coupling strength between dot-i and dot-j. After diagonalizing $\mathbf{H}^{(1)}$, we can obtain three eigenvalues $\varepsilon_-, \varepsilon_0, \varepsilon_+$, for convenience we set $\varepsilon_- < \varepsilon_0 < \varepsilon_+$, and corresponding eigenstates $|\Psi_-\rangle, |\Psi_0\rangle, |\Psi_+\rangle$. More explicitly, $|\Psi_l\rangle = \sum_i v_{li}|\Phi_i\rangle$, where $l = (-,0,+)$, $i = (1,2,3)$. The coefficients are given by the eigenvectors $\mathbf{v}_l = (v_{l1}, v_{l2}, v_{l3})$ of the $\mathbf{H}^{(1)}$.

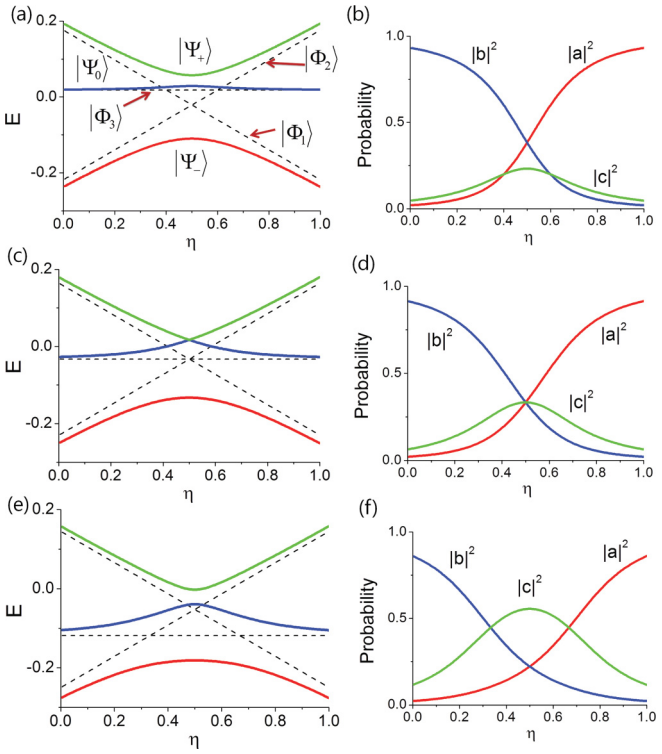

FIG. 1. (Color online) (a), (c), (e) The energy eigenvalues, $\varepsilon_-, \varepsilon_0, \varepsilon_+$ as a function of η, when $\delta = 0.05$ and $V_3 = 0.3$ (a), 0.375 (c), and 0.5 (e). (b), (d), (f) The electron distribution of the ground state ($|\Psi_-\rangle = a|\Phi_1\rangle + b|\Phi_2\rangle + c|\Phi_3\rangle$) corresponding to the red line in (a), (c), (e). The probabilities of being in dot-1 ($|a|^2$, the red line), in dot-2 ($|b|^2$, the blue line) and in dot-3 ($|c|^2$, the green line) are shown as a function of η.

Now we focus on the symmetric triple-dot case, $t_{12} = t_{23} = t_{13} = -\delta$. We take a parameter η ($0 \leqslant \eta \leqslant 1$), which corresponds to the dashed line [$V_1 = 0.75\eta, V_2 = 0.75(1-\eta)$] on the plunger gate plane (V_1, V_2) in Fig. 3(a). When $\delta = 0.05$, the single-electron eigenvalues $(\varepsilon_-, \varepsilon_0, \varepsilon_+)$ are shown, as a function of η, in Figs. 1(a), 1(c), and 1(e) for the cases of $V_3 = 0.3$, 0.375, and 0.5. The ascending, descending, and horizontal dashed lines denote the diagonal components, E_1, E_2, E_3, and correspond to independent localized states in each dot, i.e., $|\Phi_1\rangle, |\Phi_2\rangle, |\Phi_3\rangle$, respectively. Note that, as V_3 increases, the horizontal dashed line ($|\Phi_3\rangle$) is getting lower. This means that the influence of dot-3 on the ground state $|\Psi_-\rangle$ becomes stronger for larger V_3.

The influence of the dot-3 can be clearly seen in the electron distribution of the ground state ($|\Psi_-\rangle = a|\Phi_1\rangle + b|\Phi_2\rangle + c|\Phi_3\rangle$). When $V_3 = 0.3$, the crossing of E_1 and E_2 takes place below E_3 line [see the dashed lines in Fig. 1(a)]. In this case, the intermediate state ($|\Phi_3\rangle$) affects a little the ground state, resulting the small probability $|c|^2$ of finding electron in dot-3 as shown in Fig. 1(b). When E_3 line and the crossing point meet together at $\eta = 0.5$, the electron of the ground state is fully delocalized, $|a|^2 = |b|^2 = |c|^2$ [see Figs. 1(c) and 1(d)]. As V_3 increases further, the E_3 line is below the crossing point, and then the electron is mainly localized in dot-3 at $\eta = 0.5$ as shown in Figs. 1(e) and 1(f). This behavior explains the establishment and expansion of the region of $(n_1, n_2, n_3) = (0,0,1)$ charge configuration, where n_i is the electron number in dot-i, amid (0,0,0), (0,1,0), and (1,0,0) regions as shown in Figs. 3(b) and 3(c).

III. DOUBLE ELECTRON STATES

Now we consider a situation that two electrons exist in a triple-dot system. Coulomb interaction between two electrons is then newly included in the calculation of energy eigenvalues. We use a modified Hund-Milliken method.[30,31] First, we take a double-electron basis set $|\Omega_m(\mathbf{x}_1, \mathbf{x}_2)\rangle$, $m = 1,2,\ldots,8,9$,

$$|\Omega_1\rangle = |\Psi_-\Psi_-\rangle, \tag{3}$$

$$|\Omega_2\rangle = |\Psi_0\Psi_0\rangle, \tag{4}$$

$$|\Omega_3\rangle = |\Psi_+\Psi_+\rangle, \tag{5}$$

$$|\Omega_4\rangle = \frac{1}{\sqrt{2}}(|\Psi_-\Psi_0\rangle + |\Psi_0\Psi_-\rangle), \tag{6}$$

$$|\Omega_5\rangle = \frac{1}{\sqrt{2}}(|\Psi_0\Psi_+\rangle + |\Psi_+\Psi_0\rangle), \tag{7}$$

$$|\Omega_6\rangle = \frac{1}{\sqrt{2}}(|\Psi_-\Psi_+\rangle + |\Psi_+\Psi_-\rangle), \tag{8}$$

$$|\Omega_7\rangle = \frac{1}{\sqrt{2}}(|\Psi_-\Psi_0\rangle - |\Psi_0\Psi_-\rangle), \tag{9}$$

$$|\Omega_8\rangle = \frac{1}{\sqrt{2}}(|\Psi_0\Psi_+\rangle - |\Psi_+\Psi_0\rangle), \tag{10}$$

$$|\Omega_9\rangle = \frac{1}{\sqrt{2}}(|\Psi_-\Psi_+\rangle - |\Psi_+\Psi_-\rangle), \tag{11}$$

where $|\Psi_l\Psi_{l'}\rangle \equiv |\Psi_l(\mathbf{x}_1)\rangle \otimes |\Psi_{l'}(\mathbf{x}_2)\rangle$. Note that we construct the basis set by using the single-electron eigenstates $|\Psi_l\rangle$, rather than the localized orthonormal states $|\Phi_i\rangle$. This choice makes the matrix elements of double-electron Hamiltonian much simpler, since $\hat{h}(\mathbf{x})|\Psi_l\rangle = \varepsilon_l|\Psi_l\rangle$ and $\langle\Psi_l|\Psi_{l'}\rangle = 0$.

The double-electron Hamiltonian is given by

$$\mathcal{H}^{(2)} = \hat{h}(\mathbf{x}_1) + \hat{h}(\mathbf{x}_2) + C(\mathbf{x}_1, \mathbf{x}_2), \tag{12}$$

where the Coulomb potential is $C(\mathbf{x}_1, \mathbf{x}_2) = ke^2/|\mathbf{x}_1 - \mathbf{x}_2|$, e is the electron charge and $k = 1/4\pi\epsilon_0\epsilon$. The last three bases are decoupled from others, i.e., $\langle\Omega_m|\mathcal{H}^{(2)}|\Omega_n\rangle = 0$ when $m = 1,\ldots,6$ and $n = 7,8,9$, which is clear from a symmetry consideration.

Now we can evaluate the double-electron Hamiltonian matrix $\mathbf{H}^{(2)}$ whose element is $(\mathbf{H}^{(2)})_{mn} = \langle\Omega_m|\mathcal{H}^{(2)}|\Omega_n\rangle$. From the orthogonality of the single-electron eigenstates $|\Psi_l\rangle$, it is clear that the off-diagonal elements are just the matrix elements of Coulomb potential, $\langle\Omega_m|C|\Omega_n\rangle$ and the diagonal elements contain additional single-electron-eigenvalue terms.

The single-electron eigenvalue ε_l and eigenstate $|\Psi_l\rangle$ depend on the gate voltages (V_1, V_2, V_3). In the relation, $|\Psi_l\rangle = \sum_i v_{li}|\Phi_i\rangle$, the dependence is contained in the eigenvectors $\mathbf{v}_l$, and the local orthonormal state $|\Phi_i\rangle$ is assumed to be independent of the gate voltages. In order to evaluate the matrix $\mathbf{H}^{(2)}$ as a function of the gate voltages, it is necessary to set some parameters which are invariant under a gate-voltage change. This can be done by expressing the basis $|\Omega_m\rangle$ by a linear combination of two-electron states $|\Phi_i\Phi_j\rangle = |\Phi_i(\mathbf{x}_1)\rangle \otimes |\Phi_i(\mathbf{x}_2)\rangle$. Then the matrix element $\langle\Omega_m|C|\Omega_n\rangle$ can be fully characterized by additional parameters, the matrix

elements of Coulomb energy in $|\Phi_i\Phi_j\rangle$ basis set,

$$\begin{aligned} U_i &= \langle\Phi_i\Phi_i|C|\Phi_i\Phi_i\rangle, \quad i = 1,2,3, \\ X_{ij} &= \langle\Phi_i\Phi_j|C|\Phi_i\Phi_j\rangle, \quad i \neq j, \\ t^i_{ij} &= \langle\Phi_i\Phi_i|C|\Phi_i\Phi_j\rangle, \quad i \neq j, \\ g_{ij} &= \langle\Phi_i\Phi_i|C|\Phi_j\Phi_j\rangle, \quad i \neq j, \\ t^i_{jk} &= \langle\Phi_i\Phi_i|C|\Phi_j\Phi_k\rangle, \quad i \neq j \neq k, \\ f_i &= \langle\Phi_i\Phi_j|C|\Phi_i\Phi_k\rangle, \quad i \neq j \neq k, \end{aligned} \tag{13}$$

where U_i is the Coulomb energy when two electrons are together in dot-i, and X_{ij} is the Coulomb energy when one electron is in dot-i and the other is in a different dot, dot-j. The diagonal elements U_i and X_{ij} correspond to classical charging energy of dot-i and electrostatic coupling energy between dot-i and dot-j, respectively. The off-diagonal elements give very small quantum corrections in the stability diagram (see Appendix B).

IV. STABILITY DIAGRAM OF SYMMETRIC TRIPLE DOTS

Although the stability diagram of double quantum dot has been studied extensively and now well understood, a few work has been done on triple-dot stability diagrams. Here, we study a symmetric triple-dot system, i.e., $U = U_1 = U_2 = U_3$ and $X = X_{12} = X_{23} = X_{13}$ with zero off-diagonal matrix elements of the Coulomb energy in Eq. (13). Hereafter, we use values of voltage V and capacitance C with a unit voltage V_0 and a unit capacitance C_0 satisfying $C_0V_0 = |e|$, e is the electron charge, and for the energy we use the energy unit as $|e|V_0$.

For comparison, we also calculate the capacitance model with a dot capacitance $C = C_1 = C_2 = C_3 = 1$ and a mutual capacitance $C_m = C_{12} = C_{23} = C_{13} = 0.3$. For these specific capacitances, the charging energy is $E_c \simeq 0.684$ and the coupling energy is $E_m \simeq 0.158$. The capacitance model[23] is summarized in Appendix C. We take $U = E_c$ and $X = E_m$ and the diagonal element of $\mathbf{H}^{(1)}$ can be expressed by the plunger gate voltages as $E_i = -E_cV_i - E_m(V_j + V_k) + E_c/2$, where (i,j,k) are cyclic (see Appendix C for details).

First, we examine zero tunnel-coupling case $\delta = 0$ [$t_{12} = t_{23} = t_{13} = -\delta$ in Eq. (2)]. Since it is the classical limit, the resulting stability diagram is identical with the result of the classical capacitance model, as it is shown in Fig. 2. The stability diagram has a definite period $P_V = 1$ along each plunger voltage V_i since we set $C = 1$. We consider only single- and double-electron cases, so the stability domains of more than two electrons are not identified in the diagram.

It is found that the stability diagram on the intersection plane of (V_1,V_2) looks similar to that of a double-dot outside the range of $E_c/2 < V_3 < E_c/2 + 2E_m$, i.e., $0.342 < V_3 < 0.658$ for the given capacitances, but inside the range the diagram exhibits some emerging and diminishing domains. For a small $V_3(<0.342)$, all domains in the diagram have $n_3 = 0$ configuration. From $V_3 \simeq 0.342$, *triangular* regions with $n_3 = 1$ emerge at every electron-triple points, the triple point of $(n_1,n_2),(n_1+1,n_2),(n_1,n_2+1)$, and expands as shown in Figs. 2(c)–2(e).

At $V_3 = 0.5$ the diagram shows domains divided by three sets of straight lines, vertical, horizontal, and diagonal lines as shown in Fig. 2(f). The vertical and horizontal lines distinguish

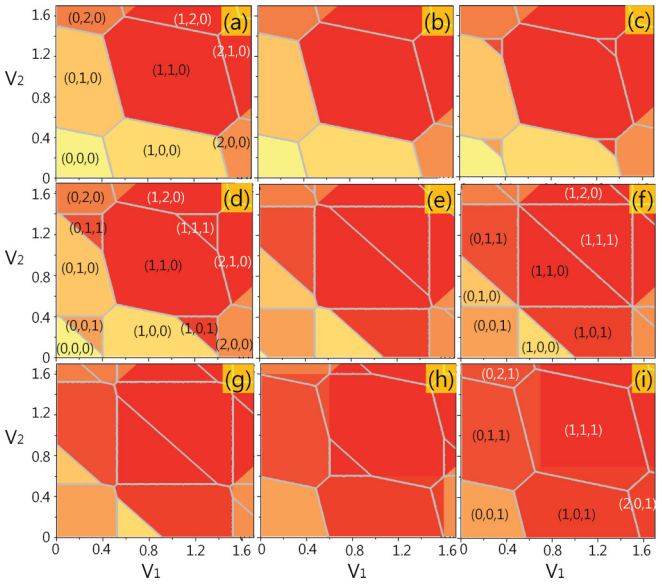

FIG. 2. (Color online) Stability diagrams of a symmetric triple-dot with zero tunnel coupling ($\delta = 0$) (presented as colored domains). The gray lines are the results of the classical capacitance model. (a) $V_3 = 0$. (b) $V_3 = 0.3$. (c) $V_3 = 0.37$. (d) $V_3 = 0.4$. (e) $V_3 = 0.48$. (f) $V_3 = 0.5$. (g) $V_3 = 0.52$. (h) $V_3 = 0.6$. (i) $V_3 = 0.7$. In the calculation, we consider only single- and double-electron configurations, so the stability domains of more than two electrons are not identified.

between different n_1 and n_2 configurations, respectively, while the diagonal line divides different n_3 configurations. An exceptional charge configuration forms at the crossing points of these three lines. At this point, six configurations are degenerated, three single-electron states $(1,0,0),(0,1,0),(0,0,1)$ and three double-electron states $(1,1,0),(1,0,1),(0,1,1)$, for example. We call this exceptional degeneracy point the *sextuple point*. The sextuple point exists only in a symmetric triangular triple-dot system, i.e., it appears when the inter-dot coupling energies are identical.

As V_3 increases further, the triangular regions with $n_3 = 0$ start to shrink toward the hole-triple points, the triple point of $(n_1,n_2),(n_1-1,n_2),(n_1,n_2-1)$, as shown in Figs. 2(g) and 2(h). Eventually, they disappear at $V_3 = 0.658$ and the stability diagram returns to that of a double-dot with $n_3 = 1$ as shown in Fig. 2(i) for $V_3 = 0.7$.

Now, we consider the stability diagram of a symmetric triple-dot *with* a finite interdot tunnel coupling δ. Main question is the effect of the tunnel coupling on the sextuple point found in the zero coupling case. The results with $\delta = 0.05$ are shown in Fig. 3. It should be emphasized that, in this finite tunnel-coupling case, exact electron-number configuration, (n_1,n_2,n_3), cannot be assigned to each domain due to the delocalization feature of the ground state. Here, we determine the number of electrons in each dot by comparing probabilities of being in each dot. For single-electron configurations, the electron is simply assigned to a dot with the highest probability. For double-electron configurations, we calculate the expectation value of electron number for each dot, p_1,p_2,p_3 ($p_1 + p_2 + p_3 = 2$). If all expectation values are less than 1, we assign two electrons to the two dots with higher expectation values. On the other hand, when one expectation

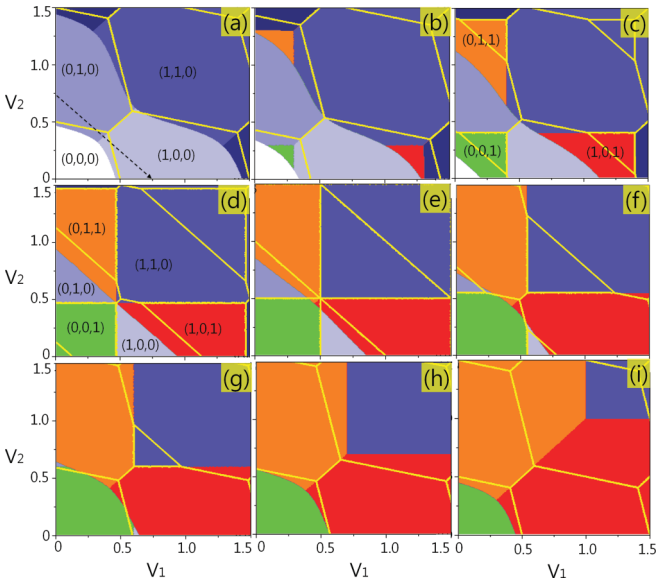

FIG. 3. (Color online) Stability diagrams of a symmetric triple-dot with a tunnel coupling $\delta = 0.05$ (presented as colored domains). The yellow lines are the results of the classical capacitance model. (a) $V_3 = 0$. (b) $V_3 = 0.3$. (c) $V_3 = 0.4$. (d) $V_3 = 0.47$. (e) $V_3 = 0.5$. (f) $V_3 = 0.55$. (g) $V_3 = 0.6$ (h) $V_3 = 0.7$ (i) $V_3 = 1.0$. The dashed arrow in (a) denotes the parameter η used in Fig. 1.

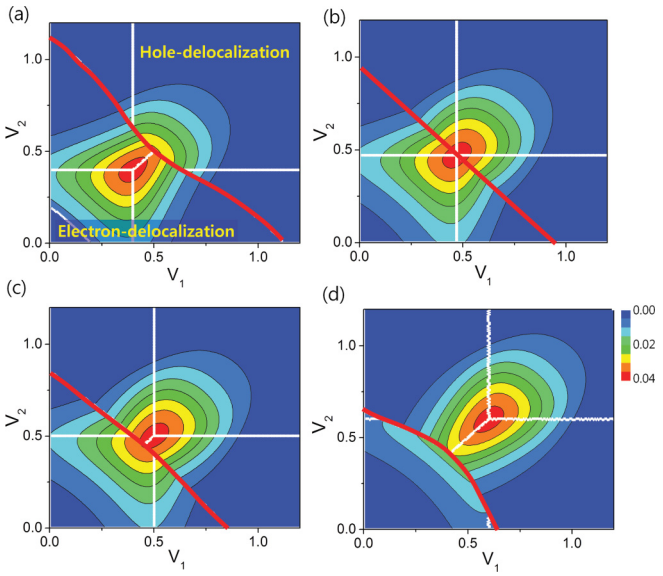

FIG. 4. (Color online) Electron- and hole-delocalization strengths (S_e and S_h) of the ground state near the quasisextuple point. (a) $V_3 = 0.4$. (b) $V_3 = 0.47$. (c) $V_3 = 0.5$. (d) $V_3 = 0.6$. The white lines denote the stability boundaries within single-electron configurations or within double-electron configurations. The red line indicates the boundary between single- and double-electron configurations.

value p_i is greater than 1, we judge the double occupancy by comparing $(p_i - 1)$ with the next higher expectation value p_j. For example, let us consider the case of $p_2 > p_1 > p_3$. Then, in the case of $p_2 < 1$, the number configuration $(n_1,n_2,n_3) = (1,1,0)$ is assigned, and for the case of $p_2 > 1$ we assign the configuration $(0,2,0)$ if $(p_2 - 1) > p_1$ and otherwise $(1,1,0)$.

At $V_3 = 0$, as shown in Fig. 3(a), the stability diagram has the rounding effect, very similar to that of a double-dot system. One distinguishable feature of tunnel-coupling effects is the early appearance of the triangular regions. From $V_3 \simeq 0.23$, the triangular regions with $n_3 = 1$ start to appear at the electron-triple points. The stability diagram at $V_3 = 0.3$, as shown in Fig. 3(b), has already well-developed $n_3 = 1$ regions, while they emerge at $V_3 = 0.342$ in the $\delta = 0$ case (yellow line). This is due to the ground-state energy pushed down by the interdot tunnel coupling, see the energy of the $|\Psi_-\rangle$ be quite below the lowest dashed lines in Fig. 1.

It is very interesting that a sextuple-like point exists at $V_3 = 0.47$, as shown in Fig. 3(d), in spite of the fact that the classical sixfold degeneracy, found at $V_3 = 0.5$, has been lifted by the tunnel coupling. In fact, the sextuple-like point is not sixfold degenerated point like the classical sextuple point, so we call it quasisextuple point. The quasisextuple point has two-fold degeneracy, single- and double-electron ground states. At each ground state an electron distributes evenly over three dots and the distribution does not change abruptly by a slight detuning of gate voltages (V_1,V_2,V_3), unlike the classical sextuple point. In Figs. 3(e)–3(i), the stabilities at $V_3 = 0.5,0.55,0.6,0.7,1.0$ are shown. We can expect that the stability diagram at $V_3 = 1.0$ [see Fig. 3(i)] would be similar to the diagram of $V_1 = 0$ [see Fig. 3(a)], except for one difference in n_3, if three-electron configurations are considered in the calculation.

In order to see delocalization of an electron near the quasi-sextuple point, we define the electron-delocalization strength S_e as the product of three local probabilities, i.e., $S_e = |a|^2|b|^2|c|^2$ for the ground state $|\Psi_-\rangle = a|\Phi_1\rangle + b|\Phi_2\rangle + c|\Phi_3\rangle$. For the double-electron configuration, we define the hole-delocalization strength as $S_h = (1 - p_1)(1 - p_2)(1 - p_3)$, p_i is the expectation value of electron number in dot-i. Figures 4(a)–4(d) shows the $S_e(V_1,V_2)$ (below the red line) and $S_h(V_1,V_2)$ (above the red line) around the quasisextuple point at $V_3 = 0.4,0.47,0.5,0.6$, respectively. It is shown that S_e displays a maximum at the electron-triple point while S_h does at the hole-triple point. At the quasisextuple point $(V_1 = V_2 = V_3 \simeq 0.47)$ both S_e and S_h are maximized as shown in Fig. 4(b), i.e., both an electron and a hole are maximally delocalized at the quasisextuple point.

It is important in practical experiments that both S_e and S_h become a maximum at the quasisextuple point, since the delocalization, over three dots, of electron and hole make it possible to maintain the characteristic feature of the sextuple point, the omnidirectional charge transfer, even for a finite tunnel-coupling case. Note that the sixfold degeneracy of the sextuple point makes the feature possible in the classical capacitance model.

The classical stability diagrams measured in the experiment[29] look different from those in Fig. 2. This can be understood by the fact that, in the real experiment, a change of V_i makes unwanted variation of E_j and E_k, as well as the desired variation of E_i. We can find some matrix describing the transform between our voltages (V_1,V_2,V_3) and the voltages (V_1',V_2',V_3') used in the experiment. Therefore the discussion related to the sextuple point is still valid in the experimental situation.

V. CONCLUSION

We have studied the effect of interdot tunnel coupling on the charge stability diagram in a symmetric triple dot. Although we discussed only on the symmetric triple-dot, our method can be directly applied to any type of triple dot if one take correctly the charging energy U_i of dot-i and the coupling energy X_{ij} between dot-i and dot-j. It is found that the sextuple point (i.e., sixfold charge configuration point) in the classical limit becomes the quasi-sextuple point at a finite tunnel coupling, where both electron- and hole-delocalizations are maximized. The delocalization of the ground state make it possible to maintain the omnidirectional charge transfer, the characteristic feature of the sextuple point. Our method can be applied to the electron transport analysis and other spin-involved quantum effects, since it describes not only the ground state, but also the excited states.

ACKNOWLEDGMENTS

We thanks H.-S. Shim and M.-S. Choi for useful discussions. S.Y.L. was supported by NRF Grant (2010-0008669) and Y.C. was partially supported by the National Research Foundation of Korea (NRF) grant (No. 2011-0003109) and the Korea Science and Engineering Foundation (KOSEF) grant (No. 2010-0000268) funded by the Korea government (MEST).

APPENDIX A: ORTHONORMAL BASIS

Here, we briefly review how to get the orthogonal basis set.[32,33] The symmetric overlap matrix $\mathbf{S}$, where $(\mathbf{S})_{ij} = s_{ij}$, can be diagonalized by an orthogonal matrix $\mathbf{U}$ as

$$\mathbf{S} = \mathbf{U}\mathbf{D}\mathbf{U}^{-1},$$

where $\mathbf{D}$ is a diagonal matrix whose elements are the eigenvalues of $\mathbf{S}$, the columns of $\mathbf{U}$ are the corresponding eigenvectors, and the inverse matrix of the orthogonal matrix $\mathbf{U}$ is given by its transpose, i.e., $\mathbf{U}^{-1} = \mathbf{U}^{T}$. The inverse square root of the overlap matrix is simply given by taking inverse square root of each diagonal elements of $\mathbf{D}$,

$$\mathbf{S}^{-1/2} = \mathbf{U}\mathbf{D}^{-1/2}\mathbf{U}^{-1},$$

where $(\mathbf{D}^{-1/2})_{ij} = \delta_{ij}/\sqrt{(\mathbf{D})_{ii}}$. If we consider a new basis set $\{|\Phi_i\rangle\}$ transformed by $\mathbf{S}^{-1/2}$ as

$$|\Phi_i\rangle = (\mathbf{S}^{-1/2})_{ij}|\phi_j\rangle, \tag{A1}$$

it is clear that the new basis set is orthogonal,

$$\langle\Phi_i|\Phi_j\rangle = \delta_{ij}.$$

APPENDIX B: MATRIX ELEMENTS OF COULOMB ENERGY

We evaluate the matrix element of Coulomb energy for a double-dot case and show the diagonal components are dominant. For an explicit calculation, we consider the S-orbital wave function

$$\phi_i(x,y) = \frac{1}{\sqrt{\pi}\sigma}\exp\left[-\frac{(x-x_i)^2+(y-y_i)^2}{2\sigma^2}\right],$$

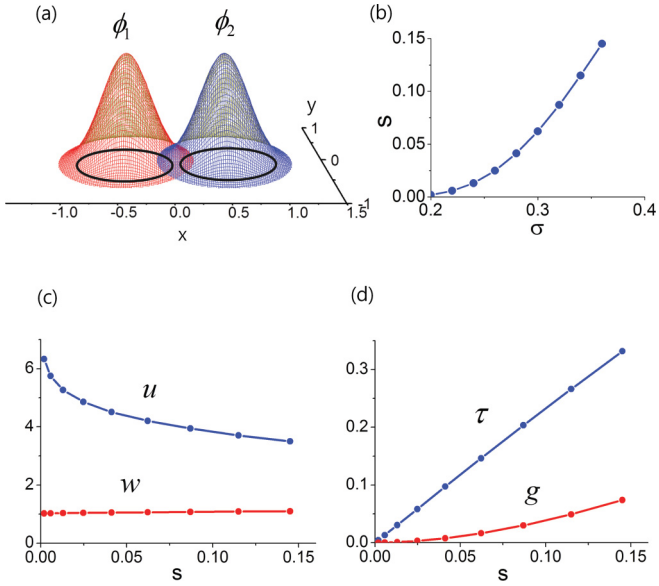

FIG. 5. (Color online) (a) Double-dot system and local wave functions ϕ_1 and ϕ_2. (b) The overlap s as a function of the wave function width σ. (c) The diagonal elements of Coulomb potential energy as a function of the overlap s. u and w. (d) The off-diagonal elements τ and g as a function of s.

where (x_i, y_i) is the center position of dot-i. We set $(x_1, y_1) = (-0.5, 0)$ and $(x_2, y_2) = (0.5, 0)$ as shown in Fig. 5(a). Since σ is the width of the wave function, the overlap $s = \langle\phi_1|\phi_2\rangle$ would increase as σ is getting larger, which is illustrated in Fig. 5(b). We calculate the matrix elements of Coulomb potential,

$$u = \langle\phi_1\phi_1|C|\phi_1\phi_1\rangle = \int d\mathbf{x}_1 d\mathbf{x}_2 |\phi_1(\mathbf{x}_1)|^2 |\phi_1(\mathbf{x}_2)|^2 \frac{ke^2}{|\mathbf{x}_1 - \mathbf{x}_2|}, \tag{B1}$$

$$w = \langle\phi_1\phi_2|C|\phi_1\phi_2\rangle = \int d\mathbf{x}_1 d\mathbf{x}_2 |\phi_1(\mathbf{x}_1)|^2 |\phi_2(\mathbf{x}_2)|^2 \frac{ke^2}{|\mathbf{x}_1 - \mathbf{x}_2|}, \tag{B2}$$

$$\tau = \langle\phi_1\phi_1|C|\phi_1\phi_2\rangle = \int d\mathbf{x}_1 d\mathbf{x}_2 |\phi_1(\mathbf{x}_1)|^2 \phi_1(\mathbf{x}_2)\phi_2(\mathbf{x}_2) \frac{ke^2}{|\mathbf{x}_1 - \mathbf{x}_2|}, \tag{B3}$$

$$g = \langle\phi_1\phi_1|C|\phi_2\phi_2\rangle = \int d\mathbf{x}_1 d\mathbf{x}_2 \phi_1(\mathbf{x}_1)\phi_2(\mathbf{x}_1)\phi_1(\mathbf{x}_2)\phi_2(\mathbf{x}_2) \frac{ke^2}{|\mathbf{x}_1 - \mathbf{x}_2|}, \tag{B4}$$

as increasing σ. The diagonal elements u and w as a function of s are shown in Fig. 5(c). The intersite Coulomb interaction energy w is almost invariant with s since the distance between dot centers is constant. The variation of off-diagonal elements τ and g are shown in Fig. 5(d). These values are small, compared to the diagonal elements u and w. In detail τ is proportional to s, i.e., $\tau \sim 2.3s$, and g is well fitted as $d \sim 4s^2$. In the numerical calculation we set $ke^2 = 1$ for convenience.

From this numerical results, we can estimate the matrix element of Coulomb energy as

$$U = \langle\Phi_i\Phi_i|C|\Phi_i\Phi_i\rangle = u + \mathcal{O}(s^2), \tag{B5}$$

$$X = \langle\Phi_1\Phi_2|C|\Phi_1\Phi_2\rangle = w + \mathcal{O}(s^2), \tag{B6}$$

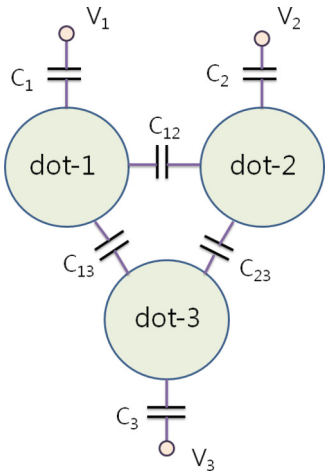

FIG. 6. (Color online) The capacitance model of a triple dot.

$$t = \langle \Phi_1 \Phi_1 | C | \Phi_1 \Phi_2 \rangle = \tau - \tfrac{1}{2}(u+w)s + \mathcal{O}(s^2), \quad \text{(B7)}$$

$$d = \langle \Phi_1 \Phi_1 | C | \Phi_2 \Phi_2 \rangle = \mathcal{O}(s^2). \quad \text{(B8)}$$

The diagonal elements of Coulomb potential in both basis sets, $|\phi_i \phi_j\rangle$ and $|\Phi_i \Phi_j\rangle$ are same up to $\mathcal{O}(s)$. In the off-diagonal elements, t has two terms, which are proportional to s. However, if we take roughly $u \simeq 4$ and $w \simeq 1$ from Fig. 5(c), the terms are mostly canceled each other as $t \simeq 2.3s - \frac{1}{2}(4+1)s \simeq -0.2s$. In the practical calculation, the effect of t is so small that the stability diagram is almost identical. Thus it is enough to consider diagonal elements U and X for the stability-diagram calculation.

APPENDIX C: THE CAPACITANCE MODEL

Here we summarize the result of the capacitance model,[23] as shown in Fig. 6, with dot capacitances C_i and mutual capcitances C_{ij}. The free energy is expressed as

$$\begin{aligned} F = {} & \frac{1}{2e^2} Q_1^{\text{eff}} \left(E_{c1} Q_1^{\text{eff}} + E_{m12} Q_2^{\text{eff}} + E_{m13} Q_3^{\text{eff}} \right) \\ & + \frac{1}{2e^2} Q_2^{\text{eff}} \left(E_{m12} Q_1^{\text{eff}} + E_{c2} Q_2^{\text{eff}} + E_{m23} Q_3^{\text{eff}} \right) \\ & + \frac{1}{2e^2} Q_3^{\text{eff}} \left(E_{m13} Q_1^{\text{eff}} + E_{m23} Q_2^{\text{eff}} + E_{c3} Q_3^{\text{eff}} \right), \end{aligned}$$

where the effective charges are

$$\begin{aligned} Q_1^{\text{eff}} &= -|e| n_1 + C_1 V_1, \\ Q_2^{\text{eff}} &= -|e| n_2 + C_2 V_2, \\ Q_3^{\text{eff}} &= -|e| n_3 + C_3 V_3, \end{aligned}$$

and the charging energies and coupling energies are

$$\begin{aligned} E_{c1} &= K\left(C_2^{\Sigma} C_3^{\Sigma} - C_{23}^2\right), \\ E_{c2} &= K\left(C_1^{\Sigma} C_3^{\Sigma} - C_{13}^2\right), \\ E_{c3} &= K\left(C_1^{\Sigma} C_2^{\Sigma} - C_{12}^2\right), \\ E_{m12} &= K\left(C_3^{\Sigma} C_{12} + C_{13} C_{23}\right), \\ E_{m23} &= K\left(C_1^{\Sigma} C_{23} + C_{12} C_{13}\right), \\ E_{m13} &= K\left(C_2^{\Sigma} C_{13} + C_{12} C_{23}\right), \end{aligned}$$

where

$$\begin{aligned} e^2/K = {} & C_1^{\Sigma} C_2^{\Sigma} C_3^{\Sigma} - 2 C_{12} C_{23} C_{13} \\ & - C_1^{\Sigma} C_{23}^2 - C_2^{\Sigma} C_{13}^2 - C_3^{\Sigma} C_{12}^2, \\ C_1^{\Sigma} = {} & C_1 + C_{12} + C_{13}, \\ C_2^{\Sigma} = {} & C_2 + C_{12} + C_{23}, \\ C_3^{\Sigma} = {} & C_3 + C_{13} + C_{23}. \end{aligned}$$

The free energy can be rearranged for electron numbers n_i as

$$\begin{aligned} F = {} & \frac{1}{2} E_{c1} n_1^2 + \frac{1}{2} E_{c2} n_2^2 + \frac{1}{2} E_{c3} n_3^2 \\ & + E_{m12} n_1 n_2 + E_{m23} n_2 n_3 + E_{m13} n_1 n_3 \\ & - \frac{1}{|e|} (E_{c1} C_1 V_1 + E_{m12} C_2 V_2 + E_{m13} C_3 V_3) n_1 \\ & - \frac{1}{|e|} (E_{m12} C_1 V_1 + E_{c2} C_2 V_2 + E_{m23} C_3 V_3) n_2 \\ & - \frac{1}{|e|} (E_{m13} C_1 V_1 + E_{m23} C_2 V_2 + E_{c3} C_3 V_3) n_3 + F_0, \end{aligned} \quad \text{(C1)}$$

where F_0 is the term independent of the electron numbers. This expression can be compared with the classical-limit energy of our theory,

$$\begin{aligned} E = {} & \sum_{i=1}^{3} \left[-\mu_i n_i + \frac{U_i}{2} n_i (n_i - 1) \right] \\ & + X_{12} n_1 n_2 + X_{23} n_2 n_3 + X_{13} n_1 n_3. \end{aligned} \quad \text{(C2)}$$

From the comparison, we know $E_{ci} = U_i$, $E_{mij} = X_{ij}$, and

$$\begin{aligned} \mu_1 &= \frac{1}{|e|} (E_{c1} C_1 V_1 + E_{m12} C_2 V_2 + E_{m13} C_3 V_3) - \frac{E_{c1}}{2}, \\ \mu_2 &= \frac{1}{|e|} (E_{m12} C_1 V_1 + E_{c2} C_2 V_2 + E_{m23} C_3 V_3) - \frac{E_{c2}}{2}, \\ \mu_3 &= \frac{1}{|e|} (E_{m13} C_1 V_1 + E_{m23} C_2 V_2 + E_{c3} C_3 V_3) - \frac{E_{c3}}{2}. \end{aligned}$$

These relations can be applied to general triple dots as well as symmetric one.

*ycchung@pusan.ac.kr

[1] C. W. J. Beenakker, Phys. Rev. B **44**, 1646 (1991).
[2] E. Leobandung, L. Guo, Y. Wang, and S. Y. Chou, Appl. Phys. Lett. **67**, 938 (1995).
[3] C. Livermore, C. H. Crouch, R. M. Westervelt, K. L. Campman, and A. C. Gossard, Science **274**, 1332 (1996).
[4] D. Goldhaber-Gordon, H. Shtrikman, D. Mahalu, D. Abusch-Magder, U. Meirav, and M. A. Kastner, Nature **391**, 156 (1998).

[5]D. Loss and D. P. DiVincenzo, Phys. Rev. A **57**, 120 (1998).
[6]F. H. L. Koppens, C. Buizert, K. J. Tielrooij, I. T. Vink, K. C. Nowack, T. Meunier, L. P. Kouwenhoven, and L. M. K. Vandersypen, Nature **442**, 766 (2006).
[7]J. R. Petta, A. C. Johnson, J. M. Taylor, E. A. Laird, A. Yacoby, M. D. Lukin, C. M. Marcus, M. P. Hanson, and A. C. Gossard, Science **309**, 2180 (2005).
[8]E. A. Laird, J. M. Taylor, D. P. DiVincenzo, C. M. Marcus, M. P. Hanson, and A. C. Gossard, Phys. Rev. B **82**, 075403 (2010).
[9]I. van Weperen, B. D. Armstrong, E. A. Laird, J. Medford, C. M. Marcus, M. P. Hanson, and A. C. Gossard, Phys. Rev. Lett. **107**, 030506 (2011).
[10]L. DiCarlo, H. J. Lynch, A. C. Johnson, L. I. Childress, K. Crockett, C. M. Marcus, M. P. Hanson, and A. C. Gossard, Phys. Rev. Lett. **92**, 226801 (2004).
[11]T. Hatano, M. Stopa, and S. Tarucha, Science **309**, 268 (2005).
[12]R. M. Potok, I. G. Rau, H. Shtrikman, Y. Oreg, and D. Goldhaber-Gordon, Nature **446**, 167 (2007).
[13]C. Emary, Phys. Rev. B **76**, 245319 (2007).
[14]C. Pöltl, C. Emary, and T. Brandes, Phys. Rev. B **80**, 115313 (2009).
[15]A. K. Mitchell and D. E. Logan, Phys. Rev. B **81**, 075126 (2010).
[16]D. S. Saraga and D. Loss, Phys. Rev. Lett. **90**, 166803 (2003).
[17]E. Vernek, C. A. Büsser, G. B. Martins, E. V. Anda, N. Sandler, and S. E. Ulloa, Phys. Rev. B **80**, 035119 (2009).
[18]R. Žitko, J. Bonča, A. Ramšak, and T. Rejec, Phys. Rev. B **73**, 153307 (2006).
[19]I. P. Gimenez, C.-Y. Hsieh, M. Korkusinski, and P. Hawrylak, Phys. Rev. B **79**, 205311 (2009).
[20]M. Stopa, Phys. Rev. Lett. **88**, 146802 (2002).
[21]A. Vidan, R. M. Westervelt, M. Stopa, M. Hanson, and A. C. Gossard, Appl. Phys. Lett. **85**, 3602 (2004).
[22]L. Gaudreau, A. S. Sachrajda, S. Studenikin, A. Kam, F. Delgado, Y. P. Shim, M. Korkusinski, and P. Hawrylak, Phys. Rev. B **80**, 075415 (2009).
[23]D. Schröer, A. D. Greentree, L. Gaudreau, K. Eberl, L. C. L. Hollenberg, J. P. Kotthaus, and S. Ludwig, Phys. Rev. B **76**, 075306 (2007).
[24]L. Gaudreau, S. A. Studenikin, A. S. Sachrajda, P. Zawadzki, A. Kam, J. Lapointe, M. Korkusinski, and P. Hawrylak, Phys. Rev. Lett. **97**, 036807 (2006).
[25]G. Granger, L. Gaudreau, A. Kam, M. Pioro-Ladriére, S. A. Studenikin, Z. R. Wasilewski, P. Zawadzki, and A. S. Sachrajda, Phys. Rev. B **82**, 075304 (2010).
[26]W. G. van der Wiel, S. De Franceschi, J. M. Elzerman, T. Fujisawa, S. Tarucha, and L. P. kouwenhoven, Rev. Mod. Phys. **75**, 1 (2003).
[27]S. Yang, X. Wang, and S. Das Sarma, Phys. Rev. B **83**, 161301(R) (2011).
[28]S. Das Sarma, X. Wang, and S. Yang, Phys. Rev. B **83**, 235314 (2011); X. Wang, S. Yang, and S. Das Sarma, *ibid.* **84**, 115301 (2011).
[29]M. Seo, H. K. Choi, S.-Y. Lee, N. Kim, Y. Chung, H.-S. Sim, V. Umansky, and D. Mahalu (unpublished).
[30]D. C. Mattis, in *The Theory of Magnetism*, Springer Series in Solid-State Sciences No. 17, Vol. 1 (Springer, New York, 1988), Sec. 4.5.
[31]G. Burkard, D. Loss, and D. P. DiVincenzo, Phys. Rev. B **59**, 2070 (1999).
[32]E. Artacho and L. Miláns del Bosch, Phys. Rev. A **43**, 5770 (1991).
[33]I. Puerto Gimenez, M. Korkusinski, and P. Hawrylak, Phys. Rev. B **76**, 075336 (2007).